TDI noises transfer functions for LISA

Dam Quang Nam and Joseph Martino
Université de Paris, CNRS, Astroparticule et Cosmologie, 75013 Paris, France

Yves Lemière
Laboratoire de Physique Corpusculaire de Caen, Université de Caen/CNRS, 14000 Caen, France

Antoine Petiteau
IRFU, CEA, Université Paris-Saclay, F-91191, Gif-sur-Yvette, France and
Université de Paris, CNRS, Astroparticule et Cosmologie, 75013 Paris, France

Jean-Baptiste Bayle
University of Glasgow, Glasgow G12 8QQ, United Kingdom

Olaf Hartwig
SYRTE, Observatoire de Paris-PSL, CNRS, Sorbonne Université, LNE, Paris, France

Martin Staab
Max Planck Institute for Gravitational Physics (Albert Einstein Institute), D-30167 Hannover, Germany and
Leibniz Universität Hannover, D-30167 Hannover, Germany

The LISA mission is the future space-based gravitational wave (GW) observatory of the European Space Agency. It is formed by 3 spacecraft exchanging laser beams in order to form multiple real and virtual interferometers. The data streams to be used in order to extract the large number and variety of GW sources are Time-Delay Interferometry (TDI) data. One important processing to produce these data is the TDI on-ground processing which recombines multiple interferometric on-board measurements to remove certain noise sources from the data such as laser frequency noise or spacecraft jitter. The LISA noise budget is therefore expressed at the TDI level in order to account for the different TDI transfer functions applied for each noise source and thus estimate their real weight on mission performance. In order to derive a usable form of these transfer functions, a model of the beams, the measurements, and TDI have been developed, and several approximation have been made. A methodology for such a derivation has been established, as well as verification procedures. It results in a set of transfer functions, which are now used by the LISA project, in particular in its performance model. Using these transfer functions, realistic noise curves for various instrumental configurations are provided to data analysis algorithms and used for instrument design.

I. INTRODUCTION

The Laser Interferometer Space Antenna (LISA) [1, 2] is a space-based gravitational wave observatory that aims to measure gravitational waves (GWs) in the millihertz range. The mission is led by ESA, with NASA as a junior partner, and European member states contributing to both hardware and processing. LISA will enable the observation of parts of the Universe invisible by other means, such as black holes and binaries of compact objects. Furthermore, we will be able to study the very early Universe soon after the Big Bang, and possibly discover yet completely unknown objects. LISA will enhance our knowledge about astrophysics, cosmology and fundamental physics.

LISA is composed of 3 Spacecraft (S/C) in heliocentric orbits, forming an equilateral triangle constellation. The constellation trajectory is in the ecliptic plane at one astronomical unit from the Sun, and leading or trailing Earth on its orbit, with an angular seperation of 10 to 30 degrees. This distance from Earth is chosen to minimize *arm-breathing* induced by the Earth while still being close enough to allow communications.

The S/C exchange laser beams to form multiple interferometers. By monitoring the changes in distance between free-falling test-masses inside the spacecraft, LISA senses gravitational waves. Six laser beams, imprinted by the gravitational waves, connecting the local and distant test-masses, interfer with local laser beams and permit measurements with picometer precision. Achieving this precision requires the suppression of many technical noise sources, the largest of which is laser frequency noise. It is expected to be several orders of magnitude above Gravitational Wave (GW) signals. Time Delay Interferometry (TDI) [3–10] will suppress this dominant source of noise by 8 orders of magnitude, bringing it below secondary noises and GW signals. The basic idea of TDI is to combine time-shifted phase or frequency measurements from the three satellites on-ground to synthesize virtual interferometers which are naturally insensitive to laser frequency noise, but still sensitive to GW signals. Other noise sources that are above the requirements [2], need to be suppressed as part of the TDI algorithm, such as clock noise. Additional algorithms are developed to

suppress these sources of noise and then integrated to the latest version of the TDI algorithm [11].

To define the instrument performances, two kinds of noises are considered: noises suppressed by TDI and unsuppressed noises. The unsuppressed noises will constitute the dominant contribution to the LISA instrument noise budget. This document will present the analytical formulation of how unsuppressed noises propagate through TDI and the validation of these formulations.

In section II, we introduce the notations and conventions used in this article (noise definitions and TDI formulation). Section III will focus on the computation methodology to get the power spectral density of the signal as a function of frequency and to compare an approximated formulation with instrument simulations performed with LISANode. The last section IV will be dedicated to the validation of the analytical noise transfer functions.

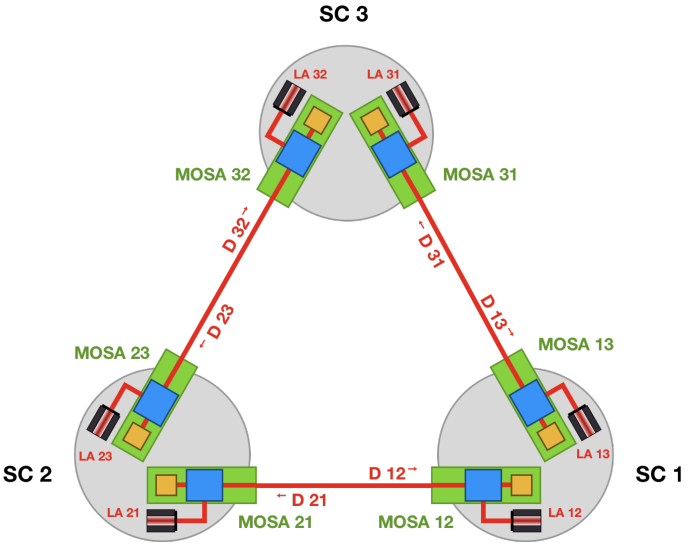

FIG. 1. LISA constellation convention. The MOSA hosted on SC1 pointing at SC2 is labeled MOSA_{12}. Each element hosted on this MOSA and the associated laser source will share the same indexes. For example the noise due to the laser associated to the MOSA_{12} will be labeled p_{12}.

II. LISA MODEL

A. Notations and conventions

In this article, we follow the convention for the LISA constellation proposed by LISA Consortium ([12]). The indexing is summarized on figure 1. Spacecraft are indexed 1, 2, 3 clockwise when looking down at their solar panels. Each of them hosts two Moving Optical Sub-Assemblies (MOSAs) which include the test-mass and its housing, the optical bench and the telescope. A laser source is associated with each MOSA. MOSAs on each spacecraft are indexed with two numbers ij:

- The first number i is the index of the S/C the MOSA is mounted on, i.e. the local S/C.
- The second number j is the index of the S/C the MOSA points to.

All subsystems of the MOSA, the associated laser and the optical measurements are indexed according to this MOSA. There are 3 main Interferometer (IFO) measurements in each MOSA: Inter-Spacecraft Interferometer (ISI), Test Mass Interferometer (TMI) and Reference Interferometer (RFI), which are respectively denoted as isi, tmi, rfi.[1]

We define $L_{ij}(t)$ as the light travel time from S/C j to S/C i, in seconds. For the propagation of light, we denote the propagation delay operator[2] by $\mathbf{D}_{ij}$, so that $\mathbf{D}_{ij}u(t) = u(t - L_{ij}(t))$ for any time-series $u(t)$. We also use the TDI delay operator $\mathcal{D}_{ij}$, such that $\mathcal{D}_{ij}u(t) = x(t - \hat{L}_{ij}(t))$, where $\hat{L}_{ij}(t)$ is the estimate of the light travel time $L_{ij}(t)$. For nested delay operators, we use the short hand notation $d_{i_1 i_2 \ldots i_n} \equiv d_{i_1 i_2} d_{i_2 i_3} \ldots d_{i_{n-1} i_n}$, where d could be $\mathbf{D}$ or $\mathcal{D}$. In general, those delay operators are not commutative since light travel times evolve with time. If we use the commutator notation of $[A, B] = AB - BA$ then $[\mathbf{D}_{ij}, \mathbf{D}_{mn}]u(t) \neq 0$ when $(i, j) \neq (m, n)$. But if delay times or armlengths are assumed to be constant, delay operators become commutative. We will use this to simplify the computation process.

Another process we indicate using an operator is the action of the anti-aliasing filters, which are used to prevent power folding in the band of interest during decimation. Its operator is denoted as $\mathcal{F}$, such as $\mathcal{F}u(t) = (f * u)(t)$, where the asterisk stands for the convolution of time-series $u(t)$ with the filter kernel $f(t)$.

The accumulated of GW contribution along the link ij (i.e., from j to i) is defined as H_{ij}.

The GW signal measured in the ISI_{ij}, caused by the accumulated delay of the beam received on S/C i from S/C j due to a GW, is labelled H_{ij}.

The wavelength of laser associated to MOSA_{ij} is λ_{ij} and its frequency is denoted as $\nu_{ij} = c/\lambda_{ij}$. We also define the frequency of the laser beam received by MOSA_{ij} from MOSA_{ji} as $\nu_{i \leftarrow j}$. Due to the Doppler shift along the link L_{ji}, $\nu_{i \leftarrow j} \neq \nu_{ji}$. The laser frequency ν is the sum of nominal frequency (carrier or sideband – THz), an offset frequency (Doppler and laser locking – MHz) and small fluctuations (noises and GWs – nHz to Hz). The interferometric signals in LISA are the heterodyne beatnote frequencies, i.e., the frequency differences between the frequencies of associated beams (offsets and small fluctuations). Their signs are (beatnote polarities)

[1] To feed the clock noise reduction algorithm, we also need the sideband measurements in the isi and the rfi [11].

[2] Technically, since the measurements will be expressed in relative frequency fluctuation units, $\mathbf{D}_{ij}$ is a Doppler-delay operator $\mathbf{D}_{ij}u(t) = (1 - \dot{L}_{ij}(t))u(t - L_{ij}(t))$ (see section 7.2 of [10]).

$\theta^{\rm isi}$ and $\theta^{\rm rfi}$ for isi and tmi / rfi signals, respectively.

$$\begin{cases} \theta^{\rm isi}_{ij} &= \text{sign}(\omega_{i\leftarrow j} - \omega_{ij}), \\ \theta^{\rm tmi}_{ij} = \theta^{\rm rfi}_{ij} &= \text{sign}(\omega_{ik} - \omega_{ij}), \end{cases} \tag{1}$$

where $\omega = 2\pi\nu$, (i,j,k) matches every permutation of $(1,2,3)$. In general, $\theta^{\rm isi}_{ij} \neq -\theta^{\rm isi}_{ji}$ but $\theta^{\rm rfi}_{ij} = -\theta^{\rm rfi}_{ik}$.

B. List of unsuppressed noises

The laser frequency noise is the dominant noise source in LISA, and suppressed by TDI post-processing algorithm (see section II G). Other noises that are not suppressed by TDI or other post-processing algorithms are called unsuppressed noises. Unsuppressed noises are subdominant (for example with respect to laser frequency noise or clock noise) but once these dominant noises have been suppressed, they contribute to the LISA noise budget. It is therefore necessary to study their propagation through TDI.

The measurements will be either in phase or frequency, or a mixture of both. The final choice is not yet made. Since the noises we are interested are expressed as small fluctuations (phase or frequency), we will assume that the measurements are in relative frequency fluctuations. It is also the unit used for most of the GW analyses.

We will denote the LISA instrumental noises as follows:

- p_{ij}: laser frequency noise (free-running or locked, see II F) of the laser on MOSA ij;
- $\delta_{ij} = \vec{\delta}_{ij}.\hat{\mathbf{n}}_{ji}/c$: projection of test-mass ij jitter noise vector $\vec{\delta}_{ij}$ onto the sensitive axis. $\hat{\mathbf{n}}_{ji}$ is the reference axis for the MOSA ij, i.e., from test-mass to Optical Bench (OB) (see figures 1 and 2). We assume that all measurements are in fractional frequency units. The test-mass jitter noise is expressed in velocity (m/s), so we need the factor $1/c$ (see [8] for the detailed derivation);
- $\Delta_{ij} = \vec{\Delta}_{ij}.\hat{\mathbf{n}}_{ji}/c$: projection of MOSA ij jitter noise vector $\vec{\Delta}_{ij}$ onto the sensitive axis (longitudinal axis);
- $N^{\rm op}_{\alpha,ij}$: generic Optical Path (OP) noise term due to optical path fluctuations on OB ij. α refers to:
  - TX/isi: OP noise on the beam transmited to the distant S/C induced by the sending S/C;
  - RX/isi: OP noise on the beam received from the distant S/C induced by the receiving S/C;
  - tmi: OP noise on adjacent beam in the TMI measurement;
  - rfi: OP noise on adjacent beam in the RFI measurement;
  - loc/isi: OP noise on local beam in the ISI measurement;
  - loc/tmi: OP noise on local beam in the TMI measurement;
  - loc/rfi: OP noise on local beam in the RFI measurement.
- $N^{ro}_{x,ij}$: readout noise for the x measurement of OB_{ij}, $x \in \{\text{isi}, \text{tmi}, \text{rfi}\}$;
- $\mu^{x}_{ij\to ik}$: backlink noise for measurement x, $x \in \{\text{tmi}, \text{rfi}\}$. This noise is dominated by straylight in the optical fibre connecting two MOSAs of the same S/C (from OB_{ij} to OB_{ik}, (i,j,k) is the set of combination of $(1,2,3)$). In general, this noise is non-reciprocal, i.e. $\mu^{x}_{ik\to ij} \neq \mu^{x}_{ij\to ik}$.

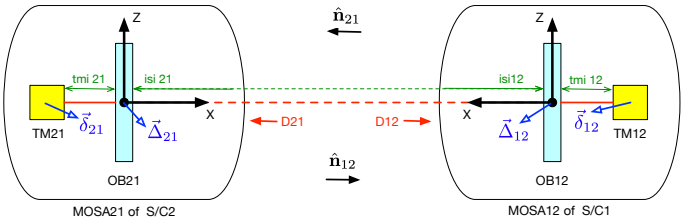

FIG. 2. Conventions for direction of beams and motions for MOSA 12 and MOSA 21. The reference X axis for MOSA 12 is equal to $\hat{\mathbf{n}}_{21}$.

C. Beam modeling

In order to model the interference measurement, we start by modeling the beams that interfere in terms of combination of noises. The main six beams of the three interferometers in the MOSA 12 are described as

$$b_{\text{isi},21\to12} = \mathbf{D}_{12}\left[p_{21} + N^{\rm op}_{TX/\text{isi},21} - \frac{1}{c}\hat{\mathbf{n}}_{12}.\vec{\Delta}_{21}\right] + H_{12} - \frac{1}{c}\hat{\mathbf{n}}_{21}.\vec{\Delta}_{12} + N^{\rm op}_{RX/\text{isi},12} \tag{2a}$$

$$b_{\text{tmi},13\to12} = p_{13} + \mu^{\rm tmi}_{13\to12} + N^{\rm op}_{\text{tmi},12} \tag{2b}$$

$$b_{\text{rfi},13\to12} = p_{13} + \mu^{\rm rfi}_{13\to12} + N^{\rm op}_{\text{rfi},12} \tag{2c}$$

$$b_{\text{isi},12\to12} = p_{12} + N^{\rm op}_{loc/\text{isi},12} \tag{2d}$$

$$b_{\text{tmi},12\to12} = p_{12} + \frac{2}{c}\hat{\mathbf{n}}_{21}.(\vec{\Delta}_{12} - \vec{\delta}_{12}) + N^{\rm op}_{loc/\text{tmi},12} \tag{2e}$$

$$b_{\text{rfi},12\to12} = p_{12} + N^{\rm op}_{loc/\text{rfi},12} \tag{2f}$$

where

- $b_{\text{isi},21\to12}$ is the beam from MOSA 21 received by MOSA 12,
- $b_{\text{rfi},13\to12}$ and $b_{\text{tmi},13\to12}$ are the beams propagating from MOSA 13 to MOSA 12 through the backlink, which respectively contribute to RFI and TMI measurements.

- $b_{x,12\to12}$ are the local beams of the MOSA 12 with $x \in \{\text{isi}, \text{tmi}, \text{rfi}\}$.

In the current design, the local beam of the tmi, $b_{\text{tmi},12\to12}$, is bouncing on the test-mass. The sign convention is such that if the test-mass moves towards the OB, i.e., $\vec{\delta}_{12}$ points in the positive direction (X of MOSA 21, $\hat{\mathbf{n}}_{21}$), the optical path on the beam $b_{\text{tmi},12\to12}$ decreases. If the OB moves away from the test-mass, i.e., $\vec{\Delta}_{12}$ points in the positive direction, the optical path on the beam $b_{\text{tmi},12\to12}$ increases while it decreases on $b_{\text{isi},21\to12}$.

The beams in MOSA 13 are constructed in the same way. One can easily write them from the formulae of MOSA 12 by replacing index 2 by 3 everywhere. The beams in the other MOSAs can be deduced by circular permutation of indices $(1 \to 2 \to 3 \to 1)$.

D. Interferometer measurement

Using those beams, we can construct the 3 main IFO measurements, for example in the MOSA 12, as follows

$$\begin{cases} \text{isi}_{12} &= \mathcal{F}\left[\theta_{12}^{\text{isi}}\left(b_{\text{isi},21\to12} - b_{\text{isi},12\to12}\right) + N_{\text{isi},12}^{ro}\right] \\ \text{tmi}_{12} &= \mathcal{F}\left[\theta_{12}^{\text{rfi}}\left(b_{\text{tmi},13\to12} - b_{\text{tmi},12\to12}\right) + N_{\text{tmi},12}^{ro}\right] \\ \text{rfi}_{12} &= \mathcal{F}\left[\theta_{12}^{\text{rfi}}\left(b_{\text{rfi},13\to12} - b_{\text{rfi},12\to12}\right) + N_{\text{rfi},12}^{ro}\right]. \end{cases} \tag{3}$$

As indicated before, the measurements are expressed in relative frequency fluctuation units. In phase units, these equations are similar, with additional conversion factors.

E. Correlations

Even though, the impact of correlations has been discussed in early TDI studies [13]. In most studies, as for example [1, 2, 14, 15], the LISA Instrument noise performance are assessed as uncorrelated single link contribution from optical measurement system and test-mass acceleration. This assumption simplifies the calculation of noise propagation but may induce non negligible errors in the estimation of LISA performances. To quantitatively estimate the deviation from the ideal case, we will consider some generic scenarios of correlation in this study. Furthermore, we can split the noises into two parts, the correlated and uncorrelated terms, and derive their transfer functions separately.

One obvious correlation scenario is related to the thermo-mechanical OP noises[3] due to the telescope. Since the same telescope is used for both sending and receiving beams, it will imprint an identical noise at Inter-spacecraft IFO's located at both end of a link. The optical path noise on the emitted beam $N_{TX/\text{isi},ij}^{OP}$ and the received beam $N_{RX/\text{isi},ij}^{OP}$ in the telescope of MOSA ij are fully correlated:

$$N_{TX/\text{isi},ij}^{OP} = N_{RX/\text{isi},ij}^{OP}. \tag{4}$$

Another correlation scenario is related to test-mass acceleration noise. The two test-masses share the same S/C and thus will likely have correlated source of noises like temperature driven noises (stiffness, symetric outgassing), cross-talk of S/C jitter, coupling with local and interplanetary magnetic fields or local gravity field fluctuation. We express it by the following correlation relation

$$\vec{\delta}_{ij}.\hat{\mathbf{n}}_{ji} = \gamma\, \vec{\delta}_{ik}.\hat{\mathbf{n}}_{ki}, \tag{5}$$

where γ is the correlation factor and (i,j,k) can be any permutation of (1,2,3). γ is 1 in the case of fully-correlated noise, or -1 in case of anti-correlation. We will derive the propagation of the fully-correlated acceleration noise in section IV. The transfer functions for fully correlated and anti-correlated acceleration noise, fully correlated and anti-correlated adjacent (same S/C) interferometer noise and fully-correlated optical path noise at the same telescope are also given (see tables II and III).

F. Frequency planning – Laser locking scheme

The inter-spacecraft separation distance varies in time due to orbital dynamics. As a consequence, the laser beam coming from the distant S/C is frequency-shifted by about 10 MHz according to the Doppler effect. The laser frequencies used for the interferometric measurement are slightly offset. There is a time evolution of the beatnote between the two beams used to measure phase shift via heterodyne interferometry.

The optical measurement system tracks the beatnote frequencies in the range of 5 to 25 MHz, which is not compatible with free running lasers and Doppler-shifted beams. To accomodate this constraint, we lock the lasers by controlling the frequency of a laser (therefore the beatnote frequencies) such that they remain equal to a pre-programmed reference value [16]. We use the RFI measurement to phase-lock a laser with its adjacent laser in the same S/C (local locking), and the ISI signal to lock the local laser to the distant laser (distant locking). In the end, 5 of 6 lasers will be locked on the primary laser. In this study, we assume that laser frequency control works perfectly so the locking beatnote offset, laser frequency offset plus the Doppler shift if it is distant locking, is exactly equal to the desired value. We also do not consider the beatnote offset in the IFO measurement, as discussed in subsection II D. The constraint equation of the beatnote fluctuation is used without filter since the

[3] While the optical path noise enters in the ifo measurements in the same way as the MOSA jitter noise, it is not cancelled by the ξ_{ij} because it does not appear in the tmi.

laser locking control loop operates at high frequency before measurements are filtered and downsampled [10].

In this study, the configuration N4-32 (cfg_N2c in [16]) has been used [4]. The detailed phase-locking is shown on figure 3. The constraints on the beatnote fluctuations are

$$\cancel{\text{isi}}_{21} = 0, \tag{6a}$$
$$\cancel{\text{rfi}}_{31} = 0, \tag{6b}$$
$$\cancel{\text{isi}}_{13} = 0, \tag{6c}$$
$$\cancel{\text{rfi}}_{12} = 0, \tag{6d}$$
$$\cancel{\text{isi}}_{23} = 0, \tag{6e}$$

which yields the following formulation for the 5 locked laser frequency fluctuations:

$$p_{23} = \theta_{23}^{\text{isi}} N_{\text{isi},23}^{ro} + b_{\text{isi},32\to23} - N_{loc/\text{isi},23}^{op}, \tag{7a}$$
$$p_{31} = \theta_{31}^{\text{rfi}} N_{\text{rfi},31}^{ro} + b_{\text{rfi},32\to31} - N_{loc/\text{rfi},31}^{op}, \tag{7b}$$
$$p_{13} = \theta_{13}^{\text{isi}} N_{\text{isi},13}^{ro} + b_{\text{isi},31\to13} - N_{loc/\text{isi},13}^{op}, \tag{7c}$$
$$p_{12} = \theta_{12}^{\text{rfi}} N_{\text{rfi},12}^{ro} + b_{\text{rfi},13\to12} - N_{loc/\text{rfi},12}^{op}, \tag{7d}$$
$$p_{21} = \theta_{21}^{\text{isi}} N_{\text{isi},21}^{ro} + b_{\text{isi},12\to21} - N_{loc/\text{isi},23}^{op}. \tag{7e}$$

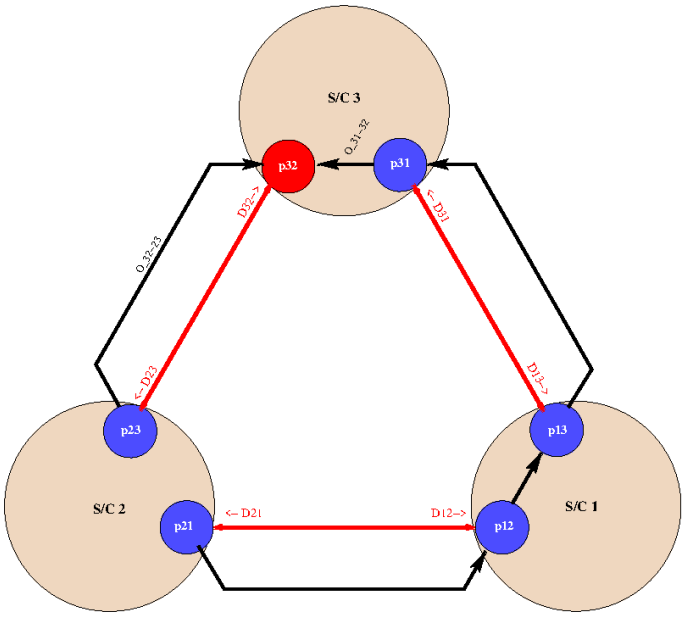

FIG. 3. Frequency planning configuration N4-32 (cfg_N2c in [16]). The primary laser is 32 with frequency fluctuations p_{32}. The other lasers are locked via RFI measurements (31 and 12) or via ISI measurements (13, 21 and 23).

[4] We used N4-32 because it was the preferred configuration when this study started. Currently the preferred configuration is N1-12 but this does not change the final results which are independent of the locking configuration.

G. Time-delay interferometry formulation

Due to the unequal armlengths entering the inter-spacecraft IFO measurements, laser noise cannot be cancelled out when two beams interferes at the photodiode. While the lasers are pre-stabilized, the laser frequency noise is still too high and will be a few orders of magnitude above the mission requirements [17]. The postprocessing algorithm called TDI will reduce the laser frequency noise below the requirements by building an equal-arm interferometer (combining time-shifted raw phase measurements). It has been showed that TDI preserves the gravitational wave signal [5, 18, 19].

The TDI formulation involves several steps, which give yield the TDI variables. The first step is to suppress the spacecraft motion (also dubbed optical bench displacement) noise Δ_{ij}.

$$\xi_{12} = \text{isi}_{12} - \theta_{12}^{\text{isi}}\theta_{12}^{\text{rfi}}\frac{\lambda_{12}}{\lambda_{21}}\frac{\text{tmi}_{12}(t) - \text{rfi}_{12}(t)}{2} - \theta_{12}^{\text{isi}}\theta_{21}^{\text{rfi}}\frac{\mathcal{D}_{12}\left[\text{tmi}_{21}(t) - \text{rfi}_{21}(t)\right]}{2}, \tag{8}$$

$$\xi_{13} = \text{isi}_{13} - \theta_{13}^{\text{isi}}\theta_{13}^{\text{rfi}}\frac{\lambda_{13}}{\lambda_{31}}\frac{\text{tmi}_{13}(t) - \text{rfi}_{13}(t)}{2} - \theta_{13}^{\text{isi}}\theta_{31}^{\text{rfi}}\frac{\mathcal{D}_{13}\left[\text{tmi}_{31}(t) - \text{rfi}_{31}(t)\right]}{2}. \tag{9}$$

Then, we can build the second intermediary variables to reduce the number of laser noises by half using the RFI measurements.

$$\eta_{12}(t) = \theta_{12}^{\text{isi}}\xi_{12}(t) + \frac{\mathcal{D}_{12}\left[\theta_{21}^{\text{rfi}}\text{rfi}_{21}(t) - \theta_{23}^{\text{rfi}}\text{rfi}_{23}(t)\right]}{2}, \tag{10}$$

$$\eta_{13}(t) = \theta_{13}^{\text{isi}}\xi_{13}(t) - \frac{\theta_{13}^{\text{rfi}}\text{rfi}_{13}(t) - \theta_{12}^{\text{rfi}}\text{rfi}_{12}(t)}{2}. \tag{11}$$

From the intermediary variables η_{ij}, we can build the TDI variables that reduce laser noise. Several TDI combinations exist [5, 9, 10, 20]. In this article, we focus on the second generation Michelson variables X_2, Y_2, Z_2, where each of the two virtual beams of the TDI Michelson [5], visits both distant spacecraft twice. We compute X_2 as

$$X_2 = (1 - \mathcal{D}_{12131})\left[(\eta_{13} + \mathcal{D}_{13}\eta_{31}) + \mathcal{D}_{131}\left(\eta_{12} + \mathcal{D}_{12}\eta_{21}\right)\right] - (1 - \mathcal{D}_{13121})\left[(\eta_{12} + \mathcal{D}_{12}\eta_{21}) + \mathcal{D}_{121}\left(\eta_{13} + \mathcal{D}_{13}\eta_{31}\right)\right]. \tag{12}$$

The other two Michelson combinations Y_2 and Z_2 are derived from this equation by circularly permuting all indices.

III. METHODOLOGY

In this section, we introduce our method to compute the TDI transfer function of the noise propagation, using as an example test-mass acceleration noise. Approximations for the simplified result are then justified. Fi-

nally, we validate the analytic transfer functions of several noises using the LISANode simulator.

A. PSD/CSD computation

We will briefly introduce a method for calculating the spectral density, which follows the procedure used in the software [21]. The Cross power Spectral Density (CSD) of two signals $u(t)$ and $v(t)$ can be defined as

$$S_{uv}(f) = CSD[u,v] = \lim_{T\to\infty} \frac{1}{T}\tilde{u}_T^*(f)\tilde{v}_T(f) \equiv \langle \tilde{u}^*(f)\tilde{v}(f)\rangle. \tag{13}$$

where $\tilde{u}(f)$ is the Fourier transform of $u(t)$ at the frequency f. $u_T(t)$ is $u(t)$ restricted to a time window of duration T. $\tilde{u}_T(f)$ is the Fourier transform of $u_T(t)$. It is obvious to show that $S_{vu}(f)$ is just the complex conjugate of $S_{uv}(f)$. The Power Spectral Density (PSD) of some stationary signal $u(t)$ is S_{uu}. It describes the energy contained in the signal $u(t)$ around the frequency f. Details on the calculation of the PSD and its statistic properties are provided in A.

To compute the Fourier transform of TDI variables, we should consider the atomic block in TDI formulation: the nested delay operator. We model the light travel times as constants, i.e. $L_{ij}(t) = L_{ij}$. For a nested delay operator applied to a timeseries, $v(t) = \mathcal{D}_{i_1 i_2 \ldots i_n} u(t)$, the Fourier transform is

$$\tilde{v}(\omega) = \exp\left(-j\omega \sum_{k=1}^{n} L_{i_k}\right) \tilde{u}(\omega). \tag{14}$$

The PSD of the usual TDI generator (X, Y and Z) are usually compositions of a limited set of patterns. For each term, we use (14) to form the Fourier transform and then compute the PSD.

We will use the short-hand notation

$$\bar{L}_{ij} = \frac{L_{ij} + L_{ji}}{2} \quad \text{and} \quad \bar{L}_{ijik} = \frac{L_{ij} + L_{ji} + L_{ik} + L_{ki}}{4} \tag{15}$$

Here, the PSD computation is done for the simple nested delay operator $\pm\left(1 - \mathcal{D}_{iji}\right) u(t)$. The list of all useful patterns is provided in table I.

$$\begin{aligned}
&\mathrm{PSD}[\pm\left(1 - \mathcal{D}_{iji}\right) u(t)]\,(\omega) \\
&\quad = \left\langle [(1 - \widetilde{\mathcal{D}_{iji}})\, u(t)](\omega) \times [(1 - \widetilde{\mathcal{D}_{iji}})\, u(t)]^*\,(\omega) \right\rangle \\
&\quad = \left\langle \left(1 - e^{-j\omega(L_{ij}+L_{ji})}\right)\left(1 - e^{j\omega(L_{ij}+L_{ji})}\right) \widetilde{u}(\omega)\widetilde{u}^*(\omega) \right\rangle \\
&\quad = 4\sin^2\left(\omega \bar{L}_{ij}\right) S_u.
\end{aligned} \tag{16}$$

The CSD computation have some common patterns. Note that we need to respect the order of the terms in the calculation.

1. $X = \pm(1 \pm \mathcal{D}_{iji})x(t)$ and $Y = \pm\left(1 \pm \mathcal{D}_{klk}\right) u(t)$. We choose one case of specific set of signs in front of the nested delay operators, the others are easily worked out in the same way.

$$\begin{aligned}
CSD\left[X,Y\right] &= CSD\left[(1 - \mathcal{D}_{iji})u(t), (1 + \mathcal{D}_{klk})\, u(t)\right] \\
&= \left\langle [(1 - \widetilde{\mathcal{D}_{iji}})\, u(t)](\omega) \times [(1 + \widetilde{\mathcal{D}_{klk}})\, u(t)]^*\,(\omega) \right\rangle \\
&= \left\langle \left(1 - e^{-2j\omega \bar{L}_{ij}}\right)\left(1 + e^{2j\omega \bar{L}_{kl}}\right) \times \widetilde{u}(\omega)\widetilde{u}^*(\omega) \right\rangle \\
&= e^{j\omega(-\bar{L}_{ij}+\bar{L}_{kl})}\left(e^{j\omega\bar{L}_{ij}} - e^{-j\omega\bar{L}_{ij}}\right) \\
&\quad \times \left(e^{-j\omega\bar{L}_{kl}} + e^{j\omega\bar{L}_{kl}}\right) \langle \widetilde{u}(\omega)\widetilde{u}^*(\omega)\rangle \\
&= e^{j\omega(-\bar{L}_{ij}+\bar{L}_{kl})} 2j\sin(\omega\bar{L}_{ij}) 2j\cos(\omega\bar{L}_{kl}) S_u \\
&= -4\sin(\omega\bar{L}_{ij})\cos(\omega\bar{L}_{kl}) e^{j\omega(-\bar{L}_{ij}+\bar{L}_{kl})} S_u
\end{aligned} \tag{17}$$

2. $X = \pm(a \pm b\mathcal{D}_{iji})x(t)$ and $Y = \pm\left(1 \pm \mathcal{D}_{klk}\right) \mathcal{D}_{i_1 i_2 \ldots i_n} u(t)$. We choose one case of specific set of signs in front of the nested delay operators, the others are easily worked out in the same way.

$$\begin{aligned}
CSD\left[X,Y\right] &= CSD\left[(a + b\mathcal{D}_{iji})u(t) * (1 - \mathcal{D}_{klk})\, \mathcal{D}_{i_1 i_2 \ldots i_n} u(t)\right] \\
&= \left\langle [(a + b\widetilde{\mathcal{D}_{iji}})\, u(t)](\omega) \right. \\
&\quad \left. \times [(1 - \mathcal{D}_{klk})\widetilde{\mathcal{D}_{i_1 i_2 \ldots i_n}} u(t)]^*\,(\omega) \right\rangle \\
&= \left\langle \left(a + be^{-j\omega(L_{ij}+L_{ji})}\right)\left(1 - e^{j\omega(L_{kl}+L_{lk})}\right) \right. \\
&\quad \left. \times\, e^{j\omega(L_{i_1}+L_{i_2}+\ldots+L_{i_n})} \widetilde{u}(\omega)\widetilde{u}^*(\omega) \right\rangle \\
&= e^{j\omega(L_{i_1}+L_{i_2}+\ldots+L_{i_n}-\bar{L}_{ij}+\bar{L}_{kl})}\left(e^{-j\omega\bar{L}_{kl}} - e^{j\omega\bar{L}_{kl}}\right) \\
&\quad \times \left(ae^{j\omega\bar{L}_{ij}} + be^{-j\omega\bar{L}_{ij}}\right) \langle \widetilde{u}(\omega)\widetilde{u}^*(\omega)\rangle \\
&= -2j\sin(\omega\bar{L}_{kl}) e^{j\omega(L_{i_1}+L_{i_2}+\ldots+L_{i_n}-\bar{L}_{ij}+\bar{L}_{kl})} \\
&\quad \times \left(ae^{j\omega\bar{L}_{ij}} + be^{-j\omega\bar{L}_{ij}}\right) S_u.
\end{aligned} \tag{18}$$

B. Approximation justification

In the previous subsections, some assumptions and approximations are made to reduce the complexity of the calculation. There are collected and justified here.

1. We assume that clock noise has been suppressed totally by the clock noise reduction algorithm [11]. Therefore we do not need to consider the sideband beams in our beam model, since they are only used for clock noise reduction. Since the residual clock noise is expected below secondary noises, this assumption is acceptable in our study case.

2. All measurements are perfectly synchronized in the Barycentric Coordinate Time. Hence, there are

Nested delay operator	PSD
$\pm\left(1-\mathcal{D}_{iji}\right)u(t)$	$4\sin^2\left(\omega\bar{L}_{ij}\right)S_u$
$\pm\left(1+\mathcal{D}_{iji}\right)u(t)$	$4\cos^2\left(\omega\bar{L}_{ij}\right)S_u$
$\pm\left(1-\mathcal{D}_{iji}\right)\mathcal{D}_{i_1i_2\ldots i_n}u(t)$	$4\sin^2\left(\omega\bar{L}_{ij}\right)S_u$
$\pm\left(1+\mathcal{D}_{iji}\right)\mathcal{D}_{i_1i_2\ldots i_n}u(t)$	$4\cos^2\left(\omega\bar{L}_{ij}\right)S_u$
$\pm\mathcal{D}_{i_1i_2\ldots i_n}\left(1-\mathcal{D}_{iji}\right)u(t)$	$4\sin^2\left(\omega\bar{L}_{ij}\right)S_u$
$\pm\mathcal{D}_{i_1i_2\ldots i_n}\left(1+\mathcal{D}_{iji}\right)u(t)$	$4\cos^2\left(\omega\bar{L}_{ij}\right)S_u$
$\pm\left(1+\mathcal{D}_{iji}\right)\left(1-\mathcal{D}_{klk}\right)u(t)$	$16\cos^2\left(\omega\bar{L}_{il}\right)\sin^2\left(\omega\bar{L}_{kl}\right)S_u$
$\pm\left(1-\mathcal{D}_{iji}\right)\left(1+\mathcal{D}_{klk}\right)u(t)$	$16\sin^2\left(\omega\bar{L}_{ij}\right)\cos^2\left(\omega\bar{L}_{kl}\right)S_u$
$\pm\left(1+\mathcal{D}_{iji}\right)\left(1+\mathcal{D}_{klk}\right)u(t)$	$16\cos^2\left(\omega\bar{L}_{ij}\right)\cos^2\left(\omega\bar{L}_{kl}\right)S_u$
$\pm\left(1-\mathcal{D}_{iji}\right)\left(1-\mathcal{D}_{klk'}\right)u(t)$	$16\sin^2\left(\omega\bar{L}_{ij}\right)\sin^2\left(\omega\bar{L}_{kl}\right)S_u$
$\pm\left(1-\mathcal{D}_{iji}-\mathcal{D}_{ijiki}+\mathcal{D}_{ikijiji}\right)u(t)$	$16\sin^2\left(\omega\bar{L}_{ij}\right)\sin^2\left(2\omega\bar{L}_{ijk}\right)S_u$
$(a\pm b\mathcal{D}_{iji})x(t)$	$\left[a^2+b^2\pm 2ab\cos\left(\omega\bar{L}_{ij}\right)\right]S_u$

TABLE I. Table of PSD for the usual patterns present in TDI time domain formulations.

no errors in time stamping the on-board measurements. This assumption simplifies the complexity of the computation.

3. All IFO measurements are expressed as fractional frequency fluctuations around the nominal laser frequency. We assume this nominal laser frequency is constant and equal for all laser source, and it is equal to the nominal laser frequency, $c/1064\text{ nm} = 282\text{ THz}$.

4. The Drag-Free Attitude Control System (DFACS) is ignored in this study, which means the S/C and test-masses are treated as independent bodies. We also neglect the tilt-to-length coupling noise in the beam model.

5. We are assuming that S/C hardware from the noise performance perspective are statistically identical. Hence 6 test-mass acceleration noises have the same PSD, or a correlation noise appearing between two adjacent test-masses will occur similarly on all S/C.

6. All armlengths of the LISA constellation are constant, and so delay operators are commutative. We use this approximation frequently with unsuppressed noises because the armlength variation is a second-order effect for these noises. Therefore, this approximation is justified in the study of unsuppressed noises.

$$L_{ij}(t) = L_{ij} \qquad \forall i,j \in \{1,2,3\} \tag{19}$$

7. Mostly in the case of unsuppressed noises, we neglect ranging and interpolation errors so the propagation delay operators and the TDI delay operators can be treated similarly, $\mathbf{D} \approx \mathcal{D}$. The effect of ranging and interpolation errors will contribute more significantly in the case of suppressed noises but this is out of the scope of this article.

8. To simplify the final transfer functions, we use the approximation of equal armlengths, which could be considered as the average armlength for long duration of the mission operation. Due to the almost equilateral configuration of the LISA constellation, we expect the average of each armlength should be not too different.

In the simulation validation studies (see section III E), the 5 first approximations (no clock jitter noise, synchronized measurements, constant nominal laser frequency, no DFACS and noises of the same kind statistically similar) are made. The validity of these approximations will not be tested here, whereas it will be for approximations 6 to 8.

C. Procedure for spectral density computation

We will now detail the calculation of the transfer functions for unsuppressed noises, using as example test-mass acceleration noise. The propagation of other unsuppressed noises are worked out in a similar way.

The calculations are performed in several steps:

1. If we consider laser frequency planning, laser noises from the locking scheme should be substituted into the beam model[5].

2. Since most of the time, we assume that noises of different types are uncorrelated, we can ignore all noises in the beams except for the one of interest. The LISA total noise transfer function is then simply the sum of all individual noise transfer functions. If a noise correlation scenario is considered, we need to apply the correlation relations and keep only one of the correlated noises in the beam model.

[5] An alternative approach is shown in section 12.2 of [10]. In principle, TDI makes sure all the p_{ij} terms are strongly suppressed, so any secondary noise terms in p_{ij} due to laser locking are suppressed alongside the laser noise. Therefore, we expect the secondary noise levels to remain identical regardless of the locking scheme, as verified by the explicit computation.

3. Next step is the computation of TDI variables, presented in subsection II G. First are the intermediary variables, then the TDI combinations. We write the result in terms of the product of nested delay operator applied to each noise, to ease the identification of patterns in the next step.

4. Hence, we can use the patterns PSD/CSD presented in subsection III A for quick computation of the spectral density of individual noise terms. The noise terms are considered uncorrelated. The correlations are treated by introducing the same noise term in multiple measurements.

5. We use the approximation of constant armlengths (19) to simplify the computation (allowing to commute delay operators). Most of the time, the PSD XX and the CSD XY are enough because we can use index permutation to deduce the other spectral densities. This apply if the beams are symmetric, so it does not for the cases with frequency planning.

6. Finally, we sum up all components and simplify the result using some approximations presented in the end of subsection III B.

D. A few examples

1. *Uncorrelated test-mass acceleration noise without laser locking*

In this section, we only consider test-mass acceleration noise. For simplicity, we omit the time dependency in the noise notation δ, but still remember that it is a time varying signal. We only consider the projection of test-mass displacement noise on the sensitive axis, δ_{ij}, since it is what enters the measurements.

Without frequency planning and correlation, the formulation of the measurements in S/C 1 are:

$$\begin{cases} \mathrm{isi}_{12} &= 0 \\ \mathrm{rfi}_{12} &= 0 \\ \mathrm{tmi}_{12} &= 2\,\mathcal{F}\,\theta_{12}^{\mathrm{rfi}}\,\delta_{12} \end{cases} \qquad \begin{cases} \mathrm{isi}_{13} &= 0 \\ \mathrm{rfi}_{13} &= 0 \\ \mathrm{tmi}_{13} &= 2\,\mathcal{F}\,\theta_{13}^{\mathrm{rfi}}\,\delta_{13} \end{cases} \tag{20}$$

We then compute the TDI intermediary variables. We neglect the ranging and interpolation errors such that the two types of delay operators are equivalent, $\mathbf{D} \approx \mathcal{D}$. Moreover, the nominal laser wavelength for every laser source is constant and equal, i.e., $\lambda_{ij} = \lambda$. Applying these approximation to equations (8), (9), (10) and (11), we get

$$\xi_{12} = -\theta_{12}^{\mathrm{isi}}\,\mathcal{F}\left(\mathcal{D}_{12}\delta_{21} + \delta_{12}\right), \tag{21}$$
$$\xi_{13} = -\theta_{13}^{\mathrm{isi}}\,\mathcal{F}\left(\mathcal{D}_{13}\delta_{31} + \delta_{13}\right), \tag{22}$$

and then

$$\eta_{12} = -\mathcal{F}\left(\mathcal{D}_{12}\delta_{21} + \delta_{12}\right), \tag{23}$$
$$\eta_{13} = -\mathcal{F}\left(\mathcal{D}_{13}\delta_{31} + \delta_{13}\right). \tag{24}$$

The Michelson combination is computed as follows, using the constant armlength approximation (19) (we can commute the delay operators with themselves and with antialiasing filter operator[6]).

$$\begin{aligned} X_2 &= \left(1 - \mathcal{D}_{12131}\right)\left[\left(\eta_{13} + \mathcal{D}_{13}\eta_{31}\right)\right. \\ &\quad \left.+\mathcal{D}_{131}\left(\eta_{12} + \mathcal{D}_{12}\eta_{21}\right)\right] - \left(1 - \mathcal{D}_{13121}\right) \\ &\quad \times\left[\left(\eta_{12} + \mathcal{D}_{12}\eta_{21}\right) + \mathcal{D}_{121}\left(\eta_{13} + \mathcal{D}_{13}\eta_{31}\right)\right] \\ &\approx \left(1 - \mathcal{D}_{12131}\right)\left[\left(1 - \mathcal{D}_{121}\right)\left(\eta_{13} + \mathcal{D}_{13}\eta_{31}\right)\right. \\ &\qquad \left.- \left(1 - \mathcal{D}_{131}\right)\left(\eta_{12} + \mathcal{D}_{12}\eta_{21}\right)\right] \\ &= \mathcal{F}\Big\{ - \left(1 - \mathcal{D}_{12131}\right)\left(1 - \mathcal{D}_{121}\right)\left(1 + \mathcal{D}_{131}\right)\delta_{13} \\ &\qquad -2\left(1 - \mathcal{D}_{12131}\right)\left(1 - \mathcal{D}_{121}\right)\mathcal{D}_{13}\delta_{31} \\ &\qquad + \left(1 - \mathcal{D}_{12131}\right)\left(1 - \mathcal{D}_{131}\right)\left(1 + \mathcal{D}_{121}\right)\delta_{12} \\ &\qquad +2\left(1 - \mathcal{D}_{12131}\right)\left(1 - \mathcal{D}_{131}\right)\mathcal{D}_{12}\delta_{21}\Big\} \end{aligned} \tag{25}$$

The Y-channel is just the index permutation of X-channel.

$$\begin{aligned} Y_2 = \mathcal{F}\Big\{ &- \left(1 - \mathcal{D}_{23212}\right)\left(1 - \mathcal{D}_{232}\right)\left(1 + \mathcal{D}_{212}\right)\delta_{21} \\ &-2\left(1 - \mathcal{D}_{23212}\right)\left(1 - \mathcal{D}_{232}\right)\mathcal{D}_{21}\delta_{12} \\ &+ \left(1 - \mathcal{D}_{23212}\right)\left(1 - \mathcal{D}_{212}\right)\left(1 + \mathcal{D}_{232}\right)\delta_{23} \\ &+2\left(1 - \mathcal{D}_{23212}\right)\left(1 - \mathcal{D}_{212}\right)\mathcal{D}_{23}\delta_{32}\Big\} \end{aligned} \tag{26}$$

The PSD of these Michelson variables can be worked out by collecting the Fourier transforms of the autocorrelation functions of each noise in each MOSA. Assuming uncorrelated noises, the cross-terms between two different noises, such as $\langle\widetilde{\delta_{12}}^{*}(f)\widetilde{\delta_{13}}(f)\rangle$, are vanishing. We can also use results from section III A for fast deduction. For example, the contribution to the PSD of X-channel $S_{XX}(f)$ of acceleration noise in MOSA 13 reads:

$$\begin{aligned} &\mathrm{PSD}\left[-\mathcal{F}\left(1 - \mathcal{D}_{12131}\right)\left(1 - \mathcal{D}_{121}\right)\left(1 + \mathcal{D}_{131}\right)\delta_{13}\right](\omega) \\ &= 64 S_{\mathcal{F}}(\omega) S_{\delta_{13}}(\omega)\sin^2\left[\omega(\bar{L}_{12} + \bar{L}_{31})\right] \\ &\quad \times \sin^2(\omega\bar{L}_{12})\cos^2(\omega\bar{L}_{31}), \end{aligned} \tag{27}$$

where $S_{\mathcal{F}}(\omega) = \langle|\tilde{\mathcal{F}}(f)|^2\rangle$ and $S_{\delta_{13}}(\omega) = \langle|\widetilde{\delta_{13}}(f)|^2\rangle$. Then, one can check that the PSD of the X-channel for the uncorrelated test-mass acceleration noise is:

$$\begin{aligned} \mathrm{S}_{\mathrm{XX}}^{\text{uncorr acc tm}}(\omega) &= 64 S_{\mathcal{F}}(\omega)\sin^2\left[\omega(\bar{L}_{12} + \bar{L}_{31})\right] \\ &\quad \times\Big\{ \sin^2(\omega\bar{L}_{12})\left[\cos^2(\omega\bar{L}_{31})S_{\delta_{13}}(\omega)\right. \\ &\quad \left.+S_{\delta_{31}}(\omega)\right] + \sin^2(\omega\bar{L}_{31}) \\ &\quad \times\left[\cos^2(\omega\bar{L}_{12})S_{\delta_{12}}(\omega) + S_{\delta_{21}}(\omega)\right]\Big\} \end{aligned} \tag{28}$$

[6] This is not true in the case of suppressed noises like laser frequency noise. In such cases, we need to take into account the non-commutation of delay operators with themselves and with filter operators [22].

The PSD of Y-channel, $\mathrm{S}_{\mathrm{YY}}^{\text{uncorr acc tm}}$, has the same form with permuted indices $\{1\to 2, 2\to 3, 3\to 1\}$. We can use the equal armlength approximations $L_{ij}=L$ and that all test-mass acceleration noises share the same PSD, $S_{\delta_{ij}}=S_\delta$, to get:

$$\begin{aligned}\mathrm{S}_{\mathrm{XX}}^{\text{uncorr acc tm}}(\omega) &= \mathrm{S}_{\mathrm{YY}}^{\text{uncorr acc tm}}(\omega)\\ &= 64\sin^2(2\omega L)\sin^2(\omega L)\left[3+\cos(2\omega L)\right]\\ &\quad\times S_{\mathcal{F}}(\omega)S_\delta(\omega) \quad (29)\end{aligned}$$

To compute the CSD between X and Y, we use the same procedure and collect the non-zero terms that have the same noise index. Note that $CSD[Y,X]=CSD[X,Y]^*$, so we only need to compute the CSD of XY. We can also use the CSD result from section III A. For example, the contribution of acceleration noise in MOSA 12 to the CSD S_{XY} reads:

$$\begin{aligned}&\mathrm{CSD}\Big[\mathcal{F}\left(1-\mathcal{D}_{12131}\right)\left(1-\mathcal{D}_{131}\right)\left(1+\mathcal{D}_{121}\right)\delta_{12}\\ &\qquad *(-2)\left(1-\mathcal{D}_{23212}\right)\left(1-\mathcal{D}_{232}\right)\mathcal{D}_{21}\delta_{12}\Big](\omega)\\ &= -64S_{\mathcal{F}}(\omega)S_{\delta_{12}}(\omega)\sin\left[\omega(\bar{L}_{12}+\bar{L}_{31})\right]\\ &\quad\times\sin\left[\omega(\bar{L}_{12}+\bar{L}_{23})\right]\sin(\omega\bar{L}_{13})\sin(\omega\bar{L}_{23})\cos(\omega\bar{L}_{12})\\ &\quad\times\exp\left[-j\omega\left(2\bar{L}_{13}-2\bar{L}_{23}+\bar{L}_{12}-L_{21}\right)\right] \quad (30)\end{aligned}$$

One can find the CSD of XY is given by

$$\begin{aligned}\mathrm{S}_{\mathrm{XY}}^{\text{uncorr acc tm}}(\omega) &= -64S_{\mathcal{F}}(\omega)\sin\left[\omega(\bar{L}_{12}+\bar{L}_{31})\right]\\ &\quad\times\sin\left[\omega(\bar{L}_{12}+\bar{L}_{23})\right]\sin(\omega\bar{L}_{13})\\ &\quad\times\sin(\omega\bar{L}_{23})\cos(\omega\bar{L}_{12})e^{-j\omega\frac{L_{12}-L_{21}}{2}}\\ &\quad\times e^{-2j\omega\left(\bar{L}_{13}-\bar{L}_{23}\right)}\left[S_{\delta_{12}}(\omega)+S_{\delta_{21}}(\omega)\right] \quad (31)\end{aligned}$$

Assuming equal armlengths and the same test-mass acceleration noise level in all MOSAs, we obtain

$$\mathrm{S}_{\mathrm{XY}}^{\text{uncorr acc tm}}(\omega) = -64S_{\mathcal{F}}(\omega)\sin^3(2\omega L)\sin(\omega L)\,S_\delta(\omega) \quad (32)$$

2. *Uncorrelated test-mass acceleration noise with laser locking*

To account for frequency planning, we need to derive the locked laser frequency fluctuations as functions of the primary laser, p_{32}, before substituting them in the beam model and IFO measurements. We use the group of equations (7) and we only keep track of the test-mass acceleration and primary laser noises,

$$p_{23} = \mathbf{D}_{12}\; p_{32} \quad (33a)$$
$$p_{31} = p_{32} \quad (33b)$$
$$p_{13} = \mathbf{D}_{21}\; p_{32} \quad (33c)$$
$$p_{12} = \mathbf{D}_{21}\; p_{32} \quad (33d)$$
$$p_{21} = \mathbf{D}_{321}\; p_{32}. \quad (33e)$$

Due to laser locking, the beams and IFO measurements are no longer symmetric for the different S/C. We therefore give the IFO signals for the whole LISA constellation

- On S/C 1:

$$\begin{cases}\mathrm{isi}_{12} &= \theta_{12}^{\mathrm{isi}}\mathcal{F}\left(\mathbf{D}_{121}-1\right)\mathbf{D}_{13}p_{32}\\ \mathrm{rfi}_{12} &= 0\\ \mathrm{tmi}_{12} &= 2\;\mathcal{F}\;\theta_{12}^{\mathrm{rfi}}\;\delta_{12}\end{cases} \quad (34)$$

$$\begin{cases}\mathrm{isi}_{13} &= 0\\ \mathrm{rfi}_{13} &= 0\\ \mathrm{tmi}_{13} &= 2\;\mathcal{F}\;\theta_{13}^{\mathrm{rfi}}\;\delta_{13}\end{cases} \quad (35)$$

- On S/C 2:

$$\begin{cases}\mathrm{isi}_{23} &= 0\\ \mathrm{rfi}_{23} &= \theta_{23}^{\mathrm{rfi}}\mathcal{F}\left(\mathbf{D}_{213}-\mathbf{D}_{23}\right)p_{32}\\ \mathrm{tmi}_{23} &= \theta_{23}^{\mathrm{rfi}}\mathcal{F}\left[\left(\mathbf{D}_{213}-\mathbf{D}_{23}\right)p_{32}+2\delta_{23}\right]\end{cases} \quad (36)$$

$$\begin{cases}\mathrm{isi}_{21} &= 0\\ \mathrm{rfi}_{21} &= \theta_{21}^{\mathrm{rfi}}\left(\mathbf{D}_{23}-\mathbf{D}_{213}\right)p_{32}\\ \mathrm{tmi}_{21} &= \theta_{21}^{\mathrm{rfi}}\mathcal{F}\left[\left(\mathbf{D}_{23}-\mathbf{D}_{213}\right)p_{32}+2\delta_{21}\right]\end{cases} \quad (37)$$

- On S/C 3:

$$\begin{cases}\mathrm{isi}_{31} &= \theta_{31}^{\mathrm{isi}}\left(\mathbf{D}_{313}-1\right)p_{32}\\ \mathrm{rfi}_{31} &= 0\\ \mathrm{tmi}_{31} &= 2\mathcal{F}\theta_{31}^{\mathrm{rfi}}\delta_{31}\end{cases} \quad (38)$$

$$\begin{cases}\mathrm{isi}_{32} &= \theta_{32}^{\mathrm{isi}}\left(\mathbf{D}_{323}-1\right)p_{32}\\ \mathrm{rfi}_{32} &= 0\\ \mathrm{tmi}_{32} &= 2\mathcal{F}\theta_{32}^{\mathrm{rfi}}\delta_{32}\end{cases} \quad (39)$$

The next step is to compute the TDI intermediary variables ξ,η. Assuming $\mathbf{D}=\mathcal{D}$, one can verify that

$$\eta_{12} = \mathcal{F}(\mathcal{D}_{123}-\mathcal{D}_{13})p_{32} - \mathcal{F}\left(\mathcal{D}_{12}\delta_{21}+\delta_{12}\right) \quad (40)$$
$$\eta_{13} = -\mathcal{F}\left(\mathcal{D}_{13}\delta_{31}+\delta_{13}\right) \quad (41)$$
$$\eta_{23} = -\mathcal{F}\left(\mathcal{D}_{23}\delta_{32}+\delta_{23}\right) \quad (42)$$
$$\eta_{21} = \mathcal{F}(\mathcal{D}_{213}-\mathcal{D}_{23})p_{32} - \mathcal{F}\left(\mathcal{D}_{21}\delta_{12}+\delta_{21}\right) \quad (43)$$
$$\eta_{31} = \mathcal{F}(\mathcal{D}_{313}-1)p_{32} - \mathcal{F}\left(\mathcal{D}_{31}\delta_{13}+\delta_{31}\right) \quad (44)$$
$$\eta_{32} = \mathcal{F}(\mathcal{D}_{323}-1)p_{32} - \mathcal{F}\left(\mathcal{D}_{32}\delta_{23}+\delta_{32}\right) \quad (45)$$

We note that, except for the terms with laser frequency noise p_{32}, all terms in η are identical to the case without laser locking. That is expected because the locking constraints (7) do not contain test-mass acceleration noise in any term. The X-channel for laser noise only is

$$\begin{aligned}X_2^{\text{p-only}} = \mathcal{F}\big[&(1-\mathcal{D}_{13121})(1-\mathcal{D}_{12131})\\ &-(1-\mathcal{D}_{12131})(1-\mathcal{D}_{13121})\big]p_{32}, \quad (46)\end{aligned}$$

which is cancelled out when we commute the TDI delay, i.e. constant delays assumption. In the end, the TDI combinations X, Y and Z in the case of laser locking for the test-mass acceleration noise are exactly the same as in the case without locking, (29) and (32).

3. Uncorrelated readout and optical path noises with laser locking

The locking constraints (7) contain readout noises, $N^{ro}_{x,ij}$, and optical path noises, $N^{op}_{loc/x,ij}$. Therefore, the situation is different from acceleration noise. Expanding η_{12} without laser locking, we get:

$$\eta_{12} = \theta^{\rm isi}_{21}\mathcal{F}N^{ro}_{s,12} - \theta^{\rm rfi}_{21}\mathcal{F}\mathcal{D}_{12}\frac{N^{ro}_{\epsilon,21} - N^{ro}_{\rm rfi,21}}{2} - \theta^{\rm rfi}_{12}\mathcal{F}\frac{N^{ro}_{\epsilon,12} - N^{ro}_{\rm rfi,12}}{2} + \theta^{\rm rfi}_{21}\mathcal{D}_{12}\mathcal{F}\frac{N^{ro}_{\rm rfi,21} + N^{ro}_{\rm rfi,23}}{2}, \tag{47}$$

while we get with laser locking:

$$\begin{aligned}\eta_{12} = {} & \theta^{\rm isi}_{12}\mathcal{F}N^{ro}_{s,12} - \theta^{\rm rfi}_{21}\mathcal{D}_{12}\mathcal{F}\frac{N^{ro}_{\epsilon,21} - N^{ro}_{\rm rfi,21}}{2} \\ & - \theta^{\rm rfi}_{12}\mathcal{F}\frac{N^{ro}_{\epsilon,12} - N^{ro}_{\rm rfi,12}}{2} + \theta^{\rm rfi}_{21}\mathcal{D}_{12}\mathcal{F}\frac{N^{ro}_{\rm rfi,21} + N^{ro}_{\rm rfi,23}}{2} \\ & - \theta^{\rm isi}_{13}\mathcal{F}N^{ro}_{s,13} + \theta^{\rm isi}_{23}\mathcal{F}\mathcal{D}_{12}N^{ro}_{s,23} \\ & - \theta^{\rm rfi}_{31}\mathcal{F}\mathcal{D}_{13}N^{ro}_{\rm rfi,31} - \theta^{\rm rfi}_{12}\mathcal{F}N^{ro}_{\rm rfi,12}\end{aligned} \tag{48}$$

We observe that laser locking introduces additional terms. These terms actually vanish at the next TDI step, when forming the variable η. Considering, for example, solely $N^{ro}_{s,13}$, we have

$$\begin{aligned}\eta_{12} &= -\theta^{\rm isi}_{13}N^{ro}_{s,13}, \\ \eta_{21} &= \theta^{\rm isi}_{13}\mathcal{D}_{21}N^{ro}_{s,13}, \\ \eta_{31} &= \theta^{\rm isi}_{13}\mathcal{D}_{31}N^{ro}_{s,13}\end{aligned}$$

Substituting in X_2 given by equation (12), we get

$$X_2 = [1 - \mathcal{D}_{121} - \mathcal{D}_{12131} + \mathcal{D}_{1312121} + (\mathcal{D}_{13121} - \mathcal{D}_{12131}) + (\mathcal{D}_{131212131} - \mathcal{D}_{121313121})]\,\theta^{\rm isi}_{13}N^{ro}_{s,13}. \tag{49}$$

Assuming that delay operators commute, the terms in parentheses disappear and we are back to the results without locking.

One can checked that we obtain the same results as for the case without locking, for all terms of readout noises and optical path noises. Finally, we find that the results are the same with and without locking for all unsuppressed noises.

4. Correlated acceleration noise

Finally, we consider the correlation scenario (5) for test-mass acceleration noise. The correlation relation is

$$\delta_{ij} = \gamma\ \delta_{ik}, \tag{50}$$

for $(i, j, k) =$ circular permutation of $(1, 2, 3)$, with γ the correlation factor and with $j \neq k$. We substitute this in the beam model and then form the IFO measurements. Since the correlated noises are in the same S/C, the IFO measurements remain symmetric (as in the uncorrelated noise case). In S/C 1, we keep only the test-mass acceleration noise from MOSA 12,

$$\begin{cases} {\rm isi}_{12} &= 0 \\ {\rm rfi}_{12} &= 0 \\ {\rm tmi}_{12} &= 2\ \mathcal{F}\ \theta^{\rm rfi}_{12}\ \delta_{12} \end{cases} \qquad \begin{cases} {\rm isi}_{13} &= 0 \\ {\rm rfi}_{13} &= 0 \\ {\rm tmi}_{13} &= 2\ \mathcal{F}\ \theta^{\rm rfi}_{13}\ \gamma\delta_{12} \end{cases} \tag{51}$$

Then, the TDI intermediary variables η for S/C 1 are

$$\eta_{12} = -\mathcal{F}\left(\gamma\mathcal{D}_{12}\delta_{23} + \delta_{12}\right), \tag{52}$$

$$\eta_{13} = -\mathcal{F}\left(\mathcal{D}_{13}\delta_{31} + \gamma\delta_{12}\right) \tag{53}$$

Applying the same procedure as for the uncorrelated case, we get the following expression for the PSD:

$$\mathrm{S}^{\rm corr\ acc\ tm}_{\rm XX}(\omega) = 32\left[3\gamma^2 + 2\gamma + 3 + (1+\gamma)^2\cos(2\omega L)\right] \times \sin^2(2\omega L)\sin^2(\omega L)\, S_{\mathcal{F}}(\omega)S_{\delta}(\omega), \tag{54}$$

and, for the CSD,

$$\mathrm{S}^{\rm corr\ acc\ tm}_{\rm XY}(\omega) = -64\left[(1+\gamma)^2\cos(2\omega L) - \gamma\right] \times \sin^2(2\omega L)\sin^2(\omega L)\, S_{\mathcal{F}}(\omega)S_{\delta}(\omega) \tag{55}$$

This example is a good illustration of the importance of correlation. Indeed, at low frequency, $\cos(2\omega L) \sim 1$, and the fully correlated case ($\gamma = 1$) is 1.5 times higher than the uncorrelated case. On the other hand, the fully anticorrelated case ($\gamma = -1$) case is 2 times lower than the uncorrelated case.

E. Validation with simulation

1. LISANode

LISANode [23] is the current official simulator of the LISA Consortium. It is a time domain simulator based on a modular structure using graphs to connect blocks and finally core components. The core components are coded in C++ and the rest (organisation of components, graph building and validation, user interface) is in python. Part of the logic and several elements are inherited from the LISACode simulator [6, 18]. LISANode takes as inputs an orbit file, a frequency plan and potentially GW files and glitch files. It simulates the noises sources, the propagation of laser beams, the interferometric measurements, the phasemeters, the clocks, etc. It produces the interferometric measurements at 16 Hz. These measurements are then filtered and downsampled at 4 Hz to produce the telemetred data (L0.5). The simulator is then connected to a processing module to apply TDI and produce any TDI variables. It has already been used in multiple studies [11, 22, 24, 25] and is described in [8, 10].

2. Numerical method for spectral estimation

The procedure to validate the transfer function of a particular type of noise (for example acceleration noise or readout noise) is the following: i) We configure the simulation for the noise to be studied, with all other noises configured to produce zeros as output; ii) From the simulated time domain data, we compute the PSD and the CSD; iii) For the same set of frequencies, we compute data from our analytical formulation; iv) We overplot the simulated and analytical PSDs or CSDs, adding for the analytical curve, the 99.73% confidence interval (3 σ for normal distribution) which is computed statistically for our Welch PSD/CSD estimates; v) The simulated points outside the confidence interval are detected. The level of agreement between analytical formulation and simulated data is estimated based on the plot and the number of points outside the confidence interval.

IV. RESULTS

A. Propagation of unsuppressed noises

1. Analytical formulations

To summarize all analytical results, we list the noises with the specific correlation and the TDI transfer function for X in table II. The results are the same for Y and Z, even with laser locking. For all these results, the equal armlengths and equal noise level approximations are used. We do not distinguish between the case with or without laser locking the results are identical for the unsuppressed noises. For the sake of brevity, we introduce two common factors in the summary table:

$$C_{XX}(\omega) = 16\sin^2(\omega L)\sin^2(2\omega L), \tag{56}$$
$$C_{XY}(\omega) = -16\sin(\omega L)\sin^3(2\omega L). \tag{57}$$

Several types of noises share the same transfer function. For some of them, it is simply because the noises enter identically in the measurement (e.g., readout ISI and optical path ISI).

There is another set of TDI variables, called A,E,T, constructed from X,Y,Z [26, 27]:

$$A = \frac{Z-X}{\sqrt{2}},\ E = \frac{X-2Y+Z}{\sqrt{6}}, T = \frac{X+Y+Z}{\sqrt{3}} \tag{58}$$

A,E,T are useful for data analysis since they have vanishing CSDs under the approximations of equal armlengths and equal noise level for the same type noises. The PSDs for A,E,T are given in table III. They combine the PSDs and CSDs of X,Y,Z as

$$S_{AA} = \frac{S_{ZZ}+S_{XX}-2\mathrm{Re}[S_{ZX}]}{2} \tag{59}$$
$$S_{EE} = \frac{S_{XX}+4S_{YY}+S_{ZZ}-2\mathrm{Re}[2S_{XY}-S_{XZ}+2S_{YZ}]}{6} \tag{60}$$
$$S_{TT} = \frac{S_{XX}+S_{YY}+S_{ZZ}+2\mathrm{Re}[S_{XY}+S_{XZ}+S_{YZ}]}{3} \tag{61}$$

and are therefore slightly more complex. We remark that while the equal arm models derived here are accurate enough to describe the GW sensitive channels X,Y,Z, as well as for the quasi-orthogonal channels A and E, it was demonstrated that this assumption is insufficient for accurately describing the behaviour of the null-channel T, in particular at low frequencies [28, 29].

2. Analytic formulations versus simulations

For the frequency range 10^{-4} to 1 Hz, the simulated and analytical PSD/CSD for TDI X have been plotted (see figures 4, 5, 6 and 7). Red lines show the analytical formulation expressions. The blue dashed lines represent the instrument response to the simulated single noises (i.e, the test-mass acceleration noise in the following example) for a duration about 3×10^5 s for uncorrelated and correlated and about 7×10^4 s for anticorrelated. The green envelope highlights the 99.73% confidence interval with respect to the analytical formulation. The width of the envelope depends on the confidence interval and on the duration of the simulation (see the difference between 6 and 4 and 5). The probability that a single point is outside of the confidence interval is around 4.5×10^{-7} in case of a perfect agreement between analytical formulation and simulation (see appendix A and equation A5).

Figures 4, 5 and 6 show a great agreement for the test-mass acceleration noise PSD in all uncorrelated, correlated and anti-correlated cases.

The confidence interval described in the appendix A is not applicable to the CSD. Nevertheless, the CSD computation shows good visual agreement with the simulated data from LISANode (see figure 7).

B. About the propagation of suppressed noises

Although this article focuses on unsuppressed noises, for the sake of completeness, we will summarize the status of transfer functions for the suppressed noises, i.e., noises suppressed by TDI, as well as the additional noises induced by this suppression.

Laser frequency noise has to be suppressed by several order of magnitude by TDI, in order to be below the required noise level [2, 17, 27] defined by the unsuppressed noises (acceleration, readout and OP). It has been the

Noise type	Correlation	PSD	CSD
test-mass acceleration	None	$4C_{XX}(\omega)\,[3+\cos(2\omega L)]$	$4C_{XY}(\omega)$
	Fully-correlated at the same S/C	$8C_{XX}(\omega)$	$-4C_{XX}(\omega)$
	Anti-correlated at the same S/C	$8C_{XX}(\omega)\,[2+\cos(2\omega L)]$	$4C_{XX}(\omega)\,[1-4\cos(\omega L)]$
Readout (TMI) and Optical Pathlength (TMI)	None	$C_{XX}(\omega)\,[3+\cos(2\omega L)]$	$C_{XY}(\omega)$
	Correlated adjacent TMI noise	$2C_{XX}(\omega)$	$-C_{XX}(\omega)$
	Anti-correlated adjacent TMI noise	$2C_{XX}(\omega)\,[2+\cos(2\omega L)]$	$C_{XX}(\omega)\,[1-4\cos(\omega L)]$
Backlink (TMI)	None	$C_{XX}(\omega)\,[3+\cos(2\omega L)]$	$C_{XY}(\omega)$
Readout (ISI and RFI) and Optical Pathlength (ISI and RFI)	None	$4C_{XX}(\omega)$	$C_{XY}(\omega)$
	Correlated adjacent IFO noise	$2C_{XX}(\omega)$	$-C_{XX}(\omega)$
	Anti-correlated adjacent IFO noise	$6C_{XX}(\omega)$	$C_{XX}(\omega)\,[1-4\cos(\omega L)]$
	Fully correlated at the same telescope	$4C_{XX}(\omega)\,[3+\cos(2\omega L)]$	$4C_{XY}(\omega)$
Backlink (RFI)	None	$4C_{XX}(\omega)$	$C_{XY}(\omega)$

TABLE II. Summary table of analytical TDI X,Y,Z transfer functions for unsuppressed noises. All results have been simplified using approximations (refer to subsection III B).

Noise type	Correlation	PSD A & E	PSD T
test-mass acceleration	None	$4C_{XX}(\omega)\,[3+2\cos(\omega L)+\cos(2\omega L)]$	$32C_{XX}(\omega)\sin^4(\frac{\omega L}{2})$
	Fully-correlated noises at the same S/C	$4C_{XX}(\omega)\,[1+2\cos(\omega L)]^2$	$64C_{XX}(\omega)\sin^4(\frac{\omega L}{2})$
	Anti-correlated at the same S/C	$12C_{XX}(\omega)$	0
Readout (TMI) and Optical Pathlength (TMI)	None	$C_{XX}(\omega)\,[3+2\cos(\omega L)+\cos(2\omega L)]$	$8C_{XX}(\omega)\sin^4(\frac{\omega L}{2})$
	Correlated adjacent TMI noise	$3C_{XX}(\omega)$	0
	Anti-correlated adjacent TMI noise	$C_{XX}(\omega)\,[1+2\cos(\omega L)]^2$	$16C_{XX}(\omega)\sin^4\left(\frac{\omega L}{2}\right)$
Backlink (TMI)	None	$C_{XX}(\omega)\,[3+2\cos(\omega L)+\cos(2\omega L)]$	$8C_{XX}(\omega)\sin^4(\frac{\omega L}{2})$
Readout (ISI and RFI) and Optical Pathlength (ISI and RFI)	None	$2C_{XX}(\omega)\,[2+\cos(\omega L)]$	$4C_{XX}(\omega)\,[1-\cos(\omega L)]$
	Correlated adjacent IFO noise	$3C_{XX}(\omega)$	0
	Anti-correlated adjacent IFO noise	$C_{XX}(\omega)\,[5+4\cos(\omega L)]$	$-8C_{XX}(\omega)\,[-1+\cos(\omega L)]$
	Fully correlated at the same telescope	$4C_{XX}(\omega)\,[3+2\cos(\omega L)+\cos(2\omega L)]$	$32C_{XX}(\omega)\sin^4(\frac{\omega L}{2})$
Backlink (RFI)	None	$2C_{XX}(\omega)\,[2+\cos(\omega L)]$	$4C_{XX}(\omega)\,[1-\cos(\omega L)]$

TABLE III. Summary table of analytical TDI A,E,T transfer functions for unsuppressed noises. All results have been simplified using approximations (refer to subsection III B).

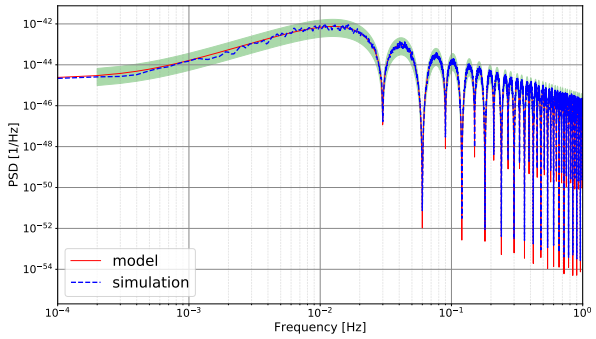

FIG. 4. Uncorrelated test-mass acceleration noise cross-comparison. The simulated data (red line) at 99.73% confidence interval (green area) are in great agreement with the analytical formulation (blue dashed line).

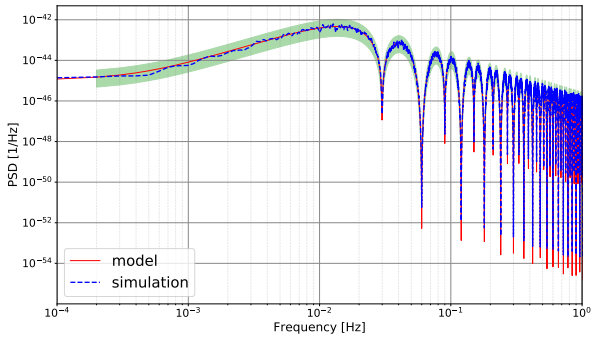

FIG. 5. Correlated test-mass acceleration noise cross-comparison. The simulated data (red line) at 99.73% confidence interval (green area) are in great agreement with the analytical formulation (blue dashed line).

main focus of TDI noise reduction studies during many years, one of the most recent studies on the topic being [22]. Because of the high level of reduction required, the residual level is sensitive to all limiting effects from the application of TDI: flexing filtering (non commutation between anti-aliasing filters and delays) [22], ranging bias, stochastic ranging (imprecision in the knowledge of delays), interpolation, aliasing and fundamental armlength mismatch (limitation due to the flexing with TDI 2.0). There are ongoing active studies on all

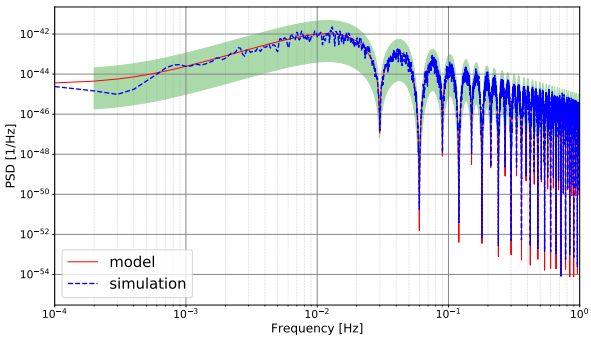

FIG. 6. Anti-correlated test-mass acceleration noise cross-comparison. The simulated data (red line) at 99.73% confidence interval (green area) are in great agreement with the analytical formulation (blue dashed line).

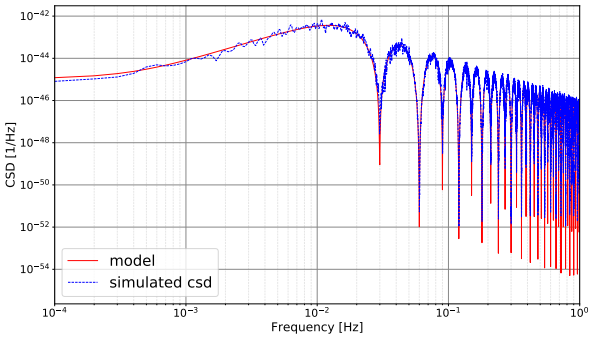

FIG. 7. CSD uncorrelated TM acceleration noise. The red line is the simulated data and the blue dashed line is the analytical formulation.

these effects and preliminary transfer functions are already available enabling to establish the expected level of the residual laser noise. Moreover, the residual laser noise depends on the laser locking configuration. Only preliminary checks based on simulation have been done and preliminary models have been developed [10], and more detailed studies are necessary.

In prinicple, most effects leading to residual laser noise will also cause residuals in other noise sources which are perfectly cancelled in an idealized situation. However, since these other suppressed noises are several orders of magnitude smaller than laser noise, their residuals can usually be neglected.

Clock noise is also reduced by TDI. While its initial level is lower than that of laser noise, it is still a few orders of magnitude higher than the required noise level. In order to suppress clock noise, the laser beams carry sideband modulation with a clock-derived signal, creating so-called clock-sidebands. Interferometric measurements of these sidebands are then used in the TDI algorithm to reduce clock noise [11].

S/C jitter noises $\vec{\Delta}_{ij}$ are in theory perfectly cancelled by TDI when forming the ξ_{ij} (see (8) and (9)). In reality, this cancellation will not be perfect and some residual noise is expected.

Finally, since the application of TDI is a numerical procedure, some numerical limitations are expected.

The estimated residuals of all suppressed noises are currently below the required level, but some contributions are not negligeable and need to be carefully studied. The laser locking will impact some of these suppressed noises and is the topic of further studies currently underway.

V. CONCLUSION

The modeling of the noises and their propagation from the measurements to the TDI variables are crucial for the LISA mission. Indeed, the TDI algorithm will reduce some noise sources while leaving others largely untouched. The impact of correlations between links can either improve or deteriorate the performance of the mission at the TDI level. We have seen this in the particular case of test mass acceleration noise, but it is also true for tilt-to-length [30] or thermo-mechanical noises. In addition, many noises related to the application of the algorithm itself, such as interpolation, clock noise residual or sideband modulation noise [11] can only be expressed at TDI level. Whether it is to establish the noise budget of the mission or to improve our understanding and knowledge of the noise for the needs of data analysis, the use of these TDI models is necessary.

The TDI variables are the main data used to extract GW signals. Therefore it is important to have a good modeling of the noise PSD and CSD for the various TDI variables in order to search for GW sources, estimate their parameters and distinguish them from the instrument noises. This last point is particularly important for the search for stochastic backgrounds which can easily be confused with noise.

A method for computing analytically the PSD and the CSD of unsuppressed noises by TDI has been presented, as well as reasonable approximations to be used. It has been applied to the main noise sources considering all uncorrelated cases, and standard cases of correlation. The analytical expressions have been provided in tables II and III for the TDI variables X,Y,Z, A, E and T. They have been validated against simulations for X,Y,Z.

The same method can be applied to any unsuppressed noises and to any TDI variables.

The transfer functions for the unsuppressed noises with laser locking are the same as the ones without laser locking. It is not necessarily the case for suppressed noises, but we leave this for future works. Actually the propagation of suppressed noises is usually more complicated.

Several studies are underway and should soon result in publications.

Appendix A: Estimation of power spectral densities

In the following we describe the procedure of estimating the power spectral density for a stochastic time series $x(t)$ of finite length T. We use the Scipy implementation of the so called "Welch's Method". It is summarized in the following steps. First, the data is divided into M segments of length L and a window function $w(t)$ is applied. Then, for each segment the Fourier transform is calculated which form independent estimates of the power spectral density as defined in (A1). Finally, the average (see (A2)) over the M segments is taken to reduce the variance.

$$\hat{S}^{(m)}(f_k) = \frac{|\tilde{x}_w^{(m)}(f_k)|^2}{L} \tag{A1}$$

$$\bar{S}(f_k) = \frac{1}{M}\sum_{m=0}^{M-1} \hat{S}^{(m)}(f_k) \tag{A2}$$

This procedure yields estimates of $\bar{S}(f_k)$ at frequencies $f_k = \Delta f k$ with k running from zero to $K = Lf_s$. The spectral resolution is given by $\Delta f = \frac{1}{L}$. In theory one could choose to average over many segments to yield a very precise estimate of the PSD. However, in reality we are faced with limited amount of data and have to trade off between low variance and high spectral resolution.

In our studies we aim to validate the analytical PSD models with simulated data. To check whether the PSD estimates $\bar{S}(f_k)$ are consistent with the model (null hypothesis) we conduct an hypothesis test. We define the confidence level γ that represents the probability that all PSD estimates are inside a given confidence interval.

$$\gamma = \prod_{k}^{K-1} \mathrm{P}\left(\bar{S}_-(f_k) \leq \bar{S}(f_k) \leq \bar{S}_+(f_k)\right) \tag{A3}$$

We reject the null hypothesis if a single estimate $\bar{S}(f_k)$ resides outside the confidence interval.

The confidence intervals $[S_-(f_k), S_+(f_k)]$ can be derived from the statistics of the PSD estimates $\bar{S}(f_k)$. It is easy to show that $\bar{S}(f_k)$ has an expectation value of

$$\mathrm{E}\{\bar{S}(f_k)\} = \frac{(|\tilde{w}|^2 * S)(f_k)}{L} \tag{A4}$$

Moreover, it has been demonstrated in [31] that $\frac{\nu\bar{S}(f_k)}{\mathrm{E}\{\bar{S}(f_k)\}}$ is χ^2_ν distributed with $\nu = 2M$ degrees of freedom. By attributing "equal confidence" to each of the K frequency bins we can write

$$\mathrm{P}\left(\bar{S}_-(f_k) \leq \bar{S}(f_k) \leq \bar{S}_+(f_k)\right) = \gamma^{\frac{1}{K}} = 1 - \alpha \tag{A5}$$

where α is the probability that the estimate resides outside the confidence interval. The limits $\bar{S}_-(f_k)$ and $\bar{S}_+(f_k)$ are constructed symmetrically such that

$$\mathrm{P}\left(\bar{S}(f_k) < \bar{S}_-(f_k)\right) = \mathrm{P}\left(\bar{S}(f_k) > \bar{S}_+(f_k)\right) = \frac{\alpha}{2} \tag{A6}$$

They can be calculated by using the χ^2_ν distributional property.

ACKNOWLEDGMENTS

The authors thank Gerhard Heinzel for the fruitful exchanges. The authors also thank the Performance Working/Expert Group and the Simulation Working/Expert Group of the LISA Consortium. This work supported by the Centre National d'Études Spatiales (CNES), the Centre National de la Recherche Scientifique (CNRS), the Université Paris Cité, the Institut de la Recherche sur les lois Fondamentales de l'Univers of the Commissariat à l'Énergie Atomique et aux énergies alternatives (CEA/IRFU) and the Observatoire de Paris. It was also supported by the Programme National GRAM of CNRS/INSU with INP and IN2P3 co-funded by CNES.

[1] P. Amaro-Seoane, H. Audley, S. Babak, J. Baker, E. Barausse, P. Bender, E. Berti, P. Binetruy, M. Born, D. Bortoluzzi, J. Camp, C. Caprini, V. Cardoso, M. Colpi, J. Conklin, N. Cornish, C. Cutler, K. Danzmann, R. Dolesi, L. Ferraioli, V. Ferroni, E. Fitzsimons, J. Gair, L. Gesa Bote, D. Giardini, F. Gibert, C. Grimani, H. Halloin, G. Heinzel, T. Hertog, M. Hewitson, K. Holley-Bockelmann, D. Hollington, M. Hueller, H. Inchauspe, P. Jetzer, N. Karnesis, C. Killow, A. Klein, B. Klipstein, N. Korsakova, S. L. Larson, J. Livas, I. Lloro, N. Man, D. Mance, J. Martino, I. Mateos, K. McKenzie, S. T. McWilliams, C. Miller, G. Mueller, G. Nardini, G. Nelemans, M. Nofrarias, A. Petiteau, P. Pivato, E. Plagnol, E. Porter, J. Reiche, D. Robertson, N. Robertson, E. Rossi, G. Russano, B. Schutz, A. Sesana, D. Shoemaker, J. Slutsky, C. F. Sopuerta, T. Sumner, N. Tamanini, I. Thorpe, M. Troebs, M. Vallisneri, A. Vecchio, D. Vetrugno, S. Vitale, M. Volonteri, G. Wanner, H. Ward, P. Wass, W. Weber, J. Ziemer, and P. Zweifel, arXiv e-prints , arXiv:1702.00786 (2017), arXiv:1702.00786 [astro-ph.IM].

[2] LISA Science Study Team, *LISA Science Requirements Document*, Requirement Document ESA-L3-EST-SCI-RS-001-i1.0 (ESA, 2018) `https://www.cosmos.esa.int/web/lisa/lisa-documents/`.

[3] F. B. Estabrook, M. Tinto, and J. W. Armstrong, Phys. Rev. D **62**, 042002 (2000).

[4] K. R. Nayak, S. Koshti, S. V. Dhurandhar, and J.-Y. Vinet, (2005), arXiv:gr-qc/0507105 [gr-qc].

[5] M. Vallisneri, Phys. Rev. D **72**, 042003 (2005), [Erratum: Phys.Rev.D 76, 109903 (2007)], arXiv:gr-qc/0504145.

[6] A. Petiteau, *DE LA SIMULATION DE LISA A L'ANALYSE DES DONNEES. Détection d'ondes gravitationnelles par interférométrie spatiale (LISA : Laser Interferometer Space Antenna)*, Theses, Université Paris-Diderot - Paris VII (2008).

[7] M. Otto, *Time-Delay Interferometry Simulations for the Laser Interferometer Space Antenna*, Ph.D. thesis, Leibniz Universität Hannover (2016).

[8] J.-B. Bayle, *Simulation and Data Analysis for LISA (Instrumental Modeling, Time-Delay Interferometry, Noise-Reduction Performance Study, and Discrimination of Transient Gravitational Signals)*, Theses, Université de Paris ; Université Paris Diderot ; Laboratoire Astroparticules et Cosmologie (2019).

[9] M. Muratore, *Time delay interferometry for LISA science and instrument characterization*, Ph.D. thesis, University of Trento (2021).

[10] O. Hartwig, *Instrumnetal modelling and noise reduction algorithms for the Laser Interferometer Space Antenna*, Ph.D. thesis, Leibniz Universität Hannover (2021).

[11] O. Hartwig and J.-B. Bayle, Phys. Rev. D **103**, 123027 (2021), arXiv:2005.02430 [astro-ph.IM].

[12] LISA Consortium, *Conventions And Nomenclature*, Tech. Rep. LISA-LCST-MIS-ST-001-i1.0 (LISA Consortium, 2021).

[13] J. Sylvestre and M. Tinto, Phys. Rev. D **68**, 102002 (2003), arXiv:gr-qc/0308085.

[14] T. Robson, N. J. Cornish, and C. Liu, Class. Quant. Grav. **36**, 105011 (2019), arXiv:1803.01944 [astro-ph.HE].

[15] S. L. Larson, W. A. Hiscock, and R. W. Hellings, Phys. Rev. D **62**, 062001 (2000), arXiv:gr-qc/9909080.

[16] Heinzel, *LISA-AEI-INST-TN-002 1.0 LISA Frequency Planning*, Technical Note LISA-AEI-INST-TN-002 (AEI, 2018).

[17] ESA Study team, (Gehler et al.), *Mission Requirement Document*, Requirement Document ESA-L3-EST-MIS-RS-001-i1.10 (ESA, 2021).

[18] A. Petiteau, G. Auger, H. Halloin, O. Jeannin, S. Pireaux, E. Plagnol, T. Regimbau, and J. Y. Vinet, AIP Conf. Proc. **873**, 633 (2006).

[19] M. Tinto and S. V. Dhurandhar, Living Rev. Rel. **17**, 6 (2014).

[20] M. Muratore, D. Vetrugno, S. Vitale, and O. Hartwig, Phys. Rev. D **105**, 023009 (2022), arXiv:2108.02738 [gr-qc].

[21] J.-B. Bayle, "Power Spectral Density python tool," `https://pypi.org/project/psd/`.

[22] J.-B. Bayle, M. Lilley, A. Petiteau, and H. Halloin, Phys. Rev. D **99**, 084023 (2019), arXiv:1811.01575 [astro-ph.IM].

[23] J.-B. Bayle, O. Hartwig, A. Petiteau, and M. Lilley, "Lisanode," (2022).

[24] J.-B. Bayle, O. Hartwig, and M. Staab, Phys. Rev. D **104**, 023006 (2021), arXiv:2103.06976 [gr-qc].

[25] O. Hartwig, J.-B. Bayle, M. Staab, A. Hees, M. Lilley, and P. Wolf, Phys. Rev. D **105**, 122008 (2022), arXiv:2202.01124 [gr-qc].

[26] T. A. Prince, M. Tinto, S. L. Larson, and J. W. Armstrong, Phys. Rev. D **66**, 122002 (2002), arXiv:gr-qc/0209039 [gr-qc].

[27] S. Babak, A. Petiteau, and M. Hewitson, (2021), arXiv:2108.01167 [astro-ph.IM].

[28] M. Muratore, O. Hartwig, D. Vetrugno, S. Vitale, and W. J. Weber, (2022), arXiv:2207.02138 [gr-qc].

[29] M. R. Adams and N. J. Cornish, Phys. Rev. D **82**, 022002 (2010), arXiv:1002.1291 [gr-qc].

[30] S. Paczkowski, R. Giusteri, M. Hewitson, N. Karnesis, E. D. Fitzsimons, G. Wanner, and G. Heinzel, Phys. Rev. D **106**, 042005 (2022).

[31] G. M. Jenkins and D. G. Watts, *Spectral Analysis and Its Applications*, Holden-Day Series in Time Series Analysis (Holden-Day, San Francisco, 1968).